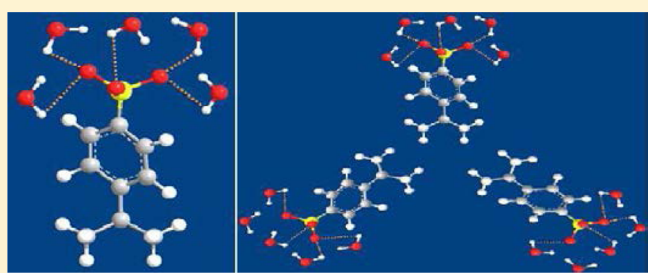


Exploring Molecular Insights into Aggregation of Hydrotrope Sodium Cumene Sulfonate in Aqueous Solution: A Molecular Dynamics Simulation Study

Shubhadip Das and Sandip Paul*

Department of Chemistry, Indian Institute of Technology, Guwahati 781039, Assam, India

ABSTRACT: Hydrotropes are an important class of molecules that enhance the solubility of an otherwise insoluble or sparingly soluble solute in water. Besides this, hydrotropes are also known to self-assemble in aqueous solution and form aggregates. It is the hydrotrope aggregate that helps in solubilizing a solute molecule in water. In view of this, we try to understand the underlying mechanism of self-aggregation of hydrotrope sodium cumene sulfonate (SCS) in water. We have carried out classical molecular dynamics simulations of aqueous SCS solutions with a regime of concentrations. Moreover, to examine the effect of temperature change on SCS aggregation, if any, we consider four different temperatures ranging from 298 to 358 K. From the estimation of densities of different solutions we calculate apparent and partial molal volumes of the hydrotrope. The changes in these quantities increase sharply at a characteristic minimum hydrotrope concentration. The determination of molal expansibility at infinite dilution for different temperatures indicates the water structure breaking by SCS molecules, which is further confirmed by the calculations of water–water pair correlation functions. In comparison with typical surfactants in micelles, a slightly lower value of volumetric change upon aggregation per carbon atom suggests the formation of a more closely packed structure of hydrotrope aggregates. A close examination of different structural properties of hydrotrope solutions reveals that the hydrophobic interactions through their hydrophobic tails significantly contribute in hydrotrope aggregation, and the dehydration of hydrophobic tail at elevated temperatures is also visible. Remarkably, the aggregates have little or no impact on the average number of water–SCS hydrogen bonds.



I. INTRODUCTION

A serious problem in designing novel drugs is their poor solubility in water. This problem has often been overcome by formulating the drugs with nontoxic, water-soluble molecules, commonly called hydrotropes.^{1–4} Almost a century ago Neuberg¹ reported that there is a large increase in the solubility of hydrophobic compounds in water upon the addition of some organic salts. This phenomenon is termed as hydrotropy, and the molecules that help in increasing the solubility of hydrophobic molecules are called hydrotropes. They can be ionic or nonionic and exist in a range of structures. Thus, hydrotropes are a special class of small amphiphilic organic molecules, and they resemble close structural features with classical surfactants as well as exhibit distinct solution properties. For example: (i) in aqueous solutions they may self-aggregate, (ii) they can act as solubilizers, and (iii) they can influence the formation of micelles and microemulsion.^{5–7} Besides acting as a solubilizers to solubilize drugs, biochemicals, and organic compounds,^{8–11} because hydrotrope additives have effectiveness in both aqueous and oil phases, they have a wide range of industrial applications, too. For example, they can be used for the extractive separation of mixtures^{12–14} as well as in cleaning, washing, antibacterials, and cosmetics purposes.¹⁵ They have catalytic property to execute organic synthetic reactions^{16,17} and are also used in paper and pulp industries.¹⁸ Moreover, in biochemistry and cell biology

they are used as protein-compatible solutes.¹⁹ Despite the fact that hydrotropes have wide range of applications, they attracted relatively little academic attention in comparison with surfactants, and the mechanism of hydrotropic actions is yet to be fully understood.

Although the classifications of hydrotropes, based on their molecular structure, are very difficult, the most studied and effective hydrotropes are alkyl benzenesulfonates based on toluene, xylene and cumene, polyhydroxybenzene, sodium salts of lower alkanols, and derivatives of aromatic acids.²⁰ Furthermore, the hydrotropic actions of aromatic hydrotropes with anionic head groups are widely studied because of the fact that for them large number of isomers are possible, and the availability of interactive π orbitals is believed to be the main reason behind their hydrotropic actions. Hydrotropes with cationic hydrophilic group, for example, salts of aromatic amines and so on, are barely studied.²¹

Although hydrotropes are usually considered as primitive amphiphiles, they have similarities and differences in terms of molecular structure and association with that of regular amphiphiles. Furthermore, despite having a polar headgroup

Received: December 10, 2014

Revised: January 15, 2015

and a hydrophobic tail, the main structural difference between a surfactant and a hydrotrope lies in the fact that the former possesses a long tail alkyl chain (C_8-C_{20}) whereas the latter has a relatively shorter alkyl chain (C_0-C_4).^{22,23} As a result, in hydrotropes a much higher hydrophile/lipophile balance (HLB) is observed as compared with that of surfactants. Thus, in order to solubilize an insoluble solute in water a relatively higher concentration level is required for hydrotropes than that of surfactants. In addition to that, some hydrotropes have been known to increase the solubility of organic solutes more than normal surfactants. As the surfactant forms a micelle above its critical micelle concentration (cmc) hydrotrope also shows aggregation behavior above minimum hydrotrope concentration (MHC).^{24,25} Analogous to surfactants, hydrotropes also reduce the surface tension of water in the region of 20 mN/m depending on their chemical structures and types.²⁶ These observations raise questions about the chemical structure regarding at what point hydrotrope becomes surfactant and when does the switch from hydrotrope to micellar behavior take place. Balasubramanian et al.²⁷ reported the results of a homologous series of sodium benzenesulfonate solutions, and they have found that the aggregation pattern in that homologous series changes somewhat sharply around sodium butyl benzenesulfonate and sodium pentyl benzenesulfonate.

Hydrotrope molecules display mild surface activity. Furthermore, although there are mostly three hypotheses (such as self-aggregation of hydrotrope molecules, hydrotrope-induced breaking of water structure, and formation of hydrotrope–solute complexes) on how hydrotropes actually enhance the solubility of hydrophobic molecules in aqueous systems, the aggregation propensity of hydrotrope molecules in aqueous solution is considered to be responsible for the enhanced solubilization of sparingly soluble other organic solutes.^{28,29} In this context it is worth noting that Booth et al.,³⁰ by employing fluctuation theory of solution (FTS), have challenged the popular belief of the role of the hydrotrope aggregates in the increased solubility of the solute. Their findings claimed that the solute–hydrotrope binding and the water activity depression are the main reasons for hydrotrope. We note that because the main goal of the present study is to explore the molecular mechanism of hydrotrope aggregation we have not used any third hydrophobic molecule. So, in the present study, it is not possible to verify the role of hydrotrope–solute interactions on hydrotrope-induced solubilization of hydrophobic molecules (as claimed by Booth et al.). Recently, Zemb and coworkers³¹ reported that hydrotropes have solubilization property, but they denied the fact that they have “weak” self-aggregation property. Nevertheless, the solubilization of hydrophobic solute in aqueous solution by the self-assembled hydrotropes is still widely accepted. Therefore, to understand the hydrotropic action of a hydrotrope, the self-aggregation of hydrotrope molecules, which is sort of a prerequisite for the increased solubility of a solute in water, needs to be clearly examined. Unfortunately, although the thermodynamic properties of medium- and long-chain surfactants are studied extensively and despite the fact that hydrotropes have been known for nearly a century, very little work has been dedicated to studying the thermodynamic properties of hydrotropes and their aggregates.^{26,27,29,32,33} As a result, the exact mechanism of hydrotrope and the structural features that make a true hydrotrope are still issues under debate. Taking together all of the research to date, on balance it appears that hydrotropes generally aggregate above MHC. However, it is very difficult to understand the microstructure of the aggregate and the details of

molecular interactions within this hydrotropic system from an experimental point of view. So to obtain better insight into the molecular details of hydrotropy, we have carried out molecular dynamics simulation of sodium cumene sulfonate (SCS) (Figure 1). Although over the last century a few experimental works have

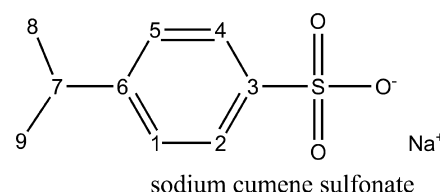


Figure 1. Structure and atomic number of sodium cumene sulfonate. Hydrogen atoms are left off for clarity.

been performed to examine the solution-state properties of hydrotropes, to best of our knowledge this is the first molecular dynamics simulation of hydrotrope molecules. Because experimentally reported MHC values of SCS are found to be inconsistent with each other,^{26,29} in this study, we first try to find out the MHC of SCS; then, by examining different structural properties, we extend our investigation toward understanding the molecular details of self-assembly process of hydrotrope SCS in water and the effect of temperature change on it.

The rest of the paper is divided into three parts. The models and simulation details are described in Section II, the results are presented and discussed in Section III, and our conclusions are briefly summarized in Section IV.

II. MODELS AND SIMULATION METHOD

Molecular dynamics simulations were performed for binary hydrotrope SCS–water mixtures at four different temperatures ranging from 298 to 358 K. For each temperature, eight different SCS concentrations were considered. Thus, altogether 32 different systems were studied. The different systems considered in this study are briefly summarized in Table 1. All simulations

Table 1.^a

system	N_{SCS}	N_{wat}	volume (nm ³)				m
			298 K	318 K	338 K	358 K	
S0	5	3600	109.08	110.31	112.33	113.59	0.077
S1	8	3600	109.83	111.28	112.89	114.44	0.123
S2	12	3600	110.25	112.46	113.45	115.57	0.185
S3	24	3600	113.38	114.65	116.00	118.59	0.370
S4	36	3600	116.43	117.86	119.90	121.80	0.556
S5	48	3600	118.80	120.48	122.54	124.33	0.741
S6	60	3600	121.95	124.03	125.52	128.18	0.926
S7	72	3600	124.92	126.58	128.40	130.79	1.111
S8	500	3600	14.89	15.16	15.44	15.70	

^a N_{SCS} and N_{wat} , respectively, are the number of sodium cumene sulfonate and water molecules. m is the molal concentration of SCS.

were performed using the AMBER12 package.³⁴ The SPC/E model was used for water molecules,³⁵ and for the cumene sulfonate group the CHARMM General Force Field (CGenFF)^{36,37} was adopted. In this study we chose the SPC/E model over TIP3P water due to the fact that when compared with the experimental results the former reproduces better structural (and dynamical) properties over the latter.³⁸ Here we note that although the use of CHARMM force field in AMBER is not a good practice, in our study the CGenFF force field was

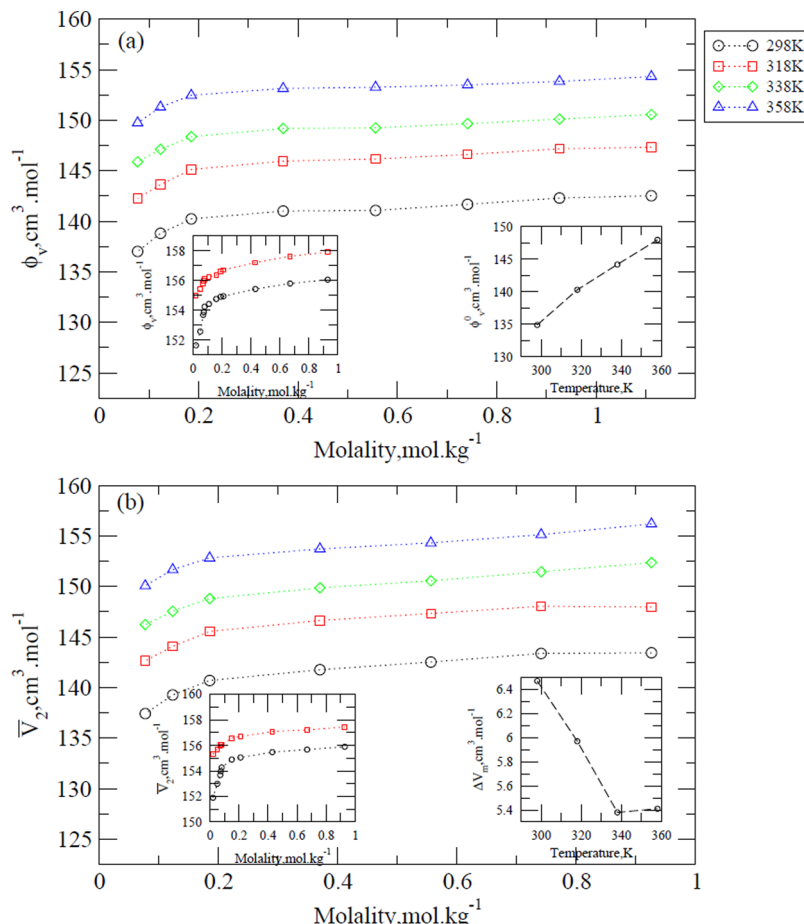


Figure 2. (a) Apparent molal volume (ϕ_v) versus concentration. Experimental apparent molal volume data (taken from ref 26) are presented in the left inset. The right inset represents the apparent molal volume at infinite dilution (ϕ_v^0) versus temperature in the present work. (b) Partial molal volume (\bar{V}_2) versus concentration. Experimental partial molal volume data (taken from ref 26) are shown in the left inset. The right inset represents the volumetric change on aggregation (ΔV_m) versus temperature in the present work.

adopted for cumene sulfonate group mainly because of the following reasons: (1) the lack of proper force field for cumene sulfonate group in AMBER and (2) the very similar functional form of the potential energy functions (in particular, for “non-biological” systems) of CHARMM and AMBER makes it possible to use the force field for the former in the latter. Indeed, using the CHAMBER toolkit³⁹ it is possible to enable the CHARMM force field in AMBER12. One Na^+ ion was added to neutralize the single negative charge carried by each sulfonate group of cumene sulfonate. The initial configurations of all systems were prepared using the PACKMOL program.⁴⁰ Furthermore, to calculate the density of pure water at different temperatures considered here, we separately carried out another four simulations for the systems containing water only, and the details of these systems are also included in Table 1. Each of these simulations was performed using cubic box, and periodic boundary conditions were applied in all three directions. At first the systems were energy for 10 000 steps, of which the first 4000 steps in steepest descent method were followed by 6000 steps in the conjugate gradient method. Thereafter, to avoid void formation, in canonical ensemble (NVT) each system was heated slowly from 0 K to the desired temperature for 320 ps at 1 atm pressure. Then, the systems were equilibrated in an isothermal–isobaric (NPT) at $P = 1.0$ atm for 5 ns. Finally, to calculate different structural properties, the production runs were performed for 40 ns in NPT ensemble. The temperature was

controlled by using the Langevin dynamics method with collision frequency of 1 ps^{-1} , and a time step of 2 fs was used. To maintain the physical pressure of each system, we used a Berendsen barostat⁴¹ with a pressure relaxation time of 2 ps. The SHAKE algorithm⁴² was used to constrain the covalent bonds between hydrogen atoms and heavy atoms, and a cutoff distance of 10 Å was defined for all nonbonded interactions. The long-ranged nonbonding interactions were treated using the particle mesh Ewald method. All pure water simulations were carried out in an NPT ensemble for 1 ns equilibration, followed by 8 ns production runs. The Ptraj program of the AMBER12 toolkit was used to analyze the trajectories obtained from the production run, and visual molecular dynamics (VMD)⁴³ was used to analyze the hydrogen-bond properties.

III. RESULTS AND DISCUSSION

A. Apparent and Partial Molal Volumes. Partial molal volume is an important thermodynamic property that provides information about the interactions between different components in a mixture as well as the local structure of the solvent. For a mixture, because the environment of the molecules changes with a change in the composition of the mixture, the partial molal volumes of the components in a mixture vary with concentration. This change in the molecular environment (and the consequent alteration of the interactions between different species) makes the thermodynamic properties of a mixture change as the

composition of the mixture is altered. In this study, because we consider a regime of temperatures, partial molal volume, which is independent of temperature (instead of partial molar volume), of SCS for different systems is calculated. The apparent and partial molal volumes of SCS for different solutions can be estimated from the density measurements.^{26,44} By using eqs 1 and 2, we have calculated apparent molal volume (ϕ_v) and partial molal volume (\bar{V}_2) of SCS from the measured densities of the aqueous SCS solutions (ρ) for different molal concentrations and temperatures.

$$\phi_v = M_2/\rho - 1000(\rho - \rho_0)/\rho\rho_0m \quad (1)$$

$$\bar{V}_2 = m(d\phi_v/dm) + \phi_v \quad (2)$$

where M_2 is the molecular weight of SCS and ρ_0 and m are the density of pure water and the molality of the solutions, respectively.

In Figure 2, we have shown how the values of ϕ_v and \bar{V}_2 change as the molality of the solution changes. At a fixed temperature, as concentration increases, prominent changes are observed in the apparent and partial molal volumes of SCS up to 0.185m concentration, indicating a major structural reorganization in the aqueous hydrotrope solutions up to this concentration. Furthermore, above 0.370m concentration, the changes in the ϕ_v and \bar{V}_2 values are not very dramatic. Because the slopes of pre- and postaggregation regions are different, the value of MHC for SCS can be estimated from this Figure. True size of the molecule and the free space between the molecules are the two components that contribute to the molal volume of hydrotrope in aqueous solution. In the context of apparent molal volume of hydrotrope, below MHC, the monomer–solvent interaction is the predominant factor, whereas the intermolecular space contributes little to it. With increasing concentration as the aggregation of hydrotropes starts, the growth of the aggregates leads to an increase in ϕ_v value of SCS, but once a critical size is attained, although the number of hydrotrope aggregates increases, the size of the aggregates should not increase much. Considering the influence of temperature on the apparent molal volumes of SCS, we find that for all of the systems considered here there is an increase in ϕ_v values with increasing temperature, and the major structural changes of hydrotrope aggregation are observed up to 0.185m, and this effect is less pronounced above 0.370m. In this context we note that our findings are in qualitative agreement with the reported experimental results (left inset of Figure 2a).²⁶ Furthermore, for all temperatures, by extrapolating the ϕ_v – m plot, we have calculated the apparent molal volume of SCS at infinite dilution (ϕ_v^0). The value of ϕ_v^0 for SCS is 134.91 cm³ mol⁻¹ at 298 K, and it increases with temperature but not exactly in linear fashion (right inset of Figure 2a). We note that our findings are in general agreement with the experimental findings,²⁶ where a nearly linear relationship between ϕ_v^0 and molality was observed. In an attempt to find out the value of molal expansibility at infinite dilution, $E_v^0 = (\partial\phi_v^0/\partial T)_p$, which gives information about how partial molal volume changes as temperature is changed, we have plotted ϕ_v^0 versus T (right inset of Figure 2a). From the slope of the graph, the value of E_v^0 is estimated to be 0.2155 cm³ K⁻¹ mol⁻¹ for SCS, whereas the reported experimental value is found to be 0.146 cm³ K⁻¹ mol⁻¹.²⁶ Here we note that for different surfactants positive molal expansibility at infinite dilution values with similar magnitudes was also previously observed.^{45,46} To get an idea about the water structure making or breaking ability of SCS molecules, we have further calculated $(\partial E_v^0/\partial T)$. This is

important because the sign of $(\partial E_v^0/\partial T)$ suggests whether the solute SCS has any structure making (if positive) or structure breaking (if negative) ability. Here we have found that $(\partial E_v^0/\partial T) = -0.0594$. Although the numerical value is not very high, the significant variation of E_v^0 with temperature gives us an idea about the water structure breaking ability of SCS molecules. This is further confirmed from O_w–O_w radial distribution functions (rdf's) for different systems that we discuss later.

The changes in partial molal volumes can give a perception about the changes in aggregation pattern of hydrotropes. Similar to apparent molal volume, the partial molal volume of SCS also increases with an increase in molality of the solution (see Figure 2b), and the increase is more rapid (and in a linear fashion) up to 0.185m concentration, but above 0.370m concentration, the changes in the \bar{V}_2 values with molality of the solution are not that remarkable. These observations imply fewer further structural changes in the aggregates above this concentration. Taking into consideration the effect of temperature on partial molal volumes of SCS, we observe an increase in \bar{V}_2 values with increasing temperature for all of the systems considered here, but the major structural changes are observed up to 0.185m, and this effect is less prominent after 0.370m. A comparison between our findings and the available experimental \bar{V}_2 values²⁶ (left inset of Figure 2b) reveals that the results obtained in this study are in qualitative accordance with the experimental findings.

Knowing the partial molal volumes in the aggregated state (\bar{V}_2^m) and singly dispersed state (\bar{V}_2^s), we further, calculate the volumetric change on aggregation $\Delta V_m = \bar{V}_2^m - \bar{V}_2^s$. For a particular system, the partial molal volume in the singly dispersed state (\bar{V}_2^s) is estimated by extrapolating to $m = 0$ concentration of the \bar{V}_2 – m plot. The ΔV_m for SCS is found to be 6.47 cm³ mol⁻¹ at 298 K, and its value decreases with an increase in temperature up to 338 K, and after that it remains constant. The same is presented in Figure 2b (right inset). The ΔV_m values are within the range of 6.47 to 5.38 cm³ mol⁻¹, and these values are very similar to those already reported values for typical surfactants.⁴⁷ Moreover, we have also calculated the value for change in ΔV_m with respect to the number of carbon atoms within the hydrotrope molecule (n), and the value of $\Delta V_m/n$ for SCS is 0.719 cm³ mol⁻¹, whereas typical values of $\Delta V_m/n$ reported for sodium octyl sulfate, sodium decyl sulfate, and sodium dodecyl sulfate, respectively, are 0.78, 0.91, and 0.9 cm³ mol⁻¹.⁴⁷ These findings suggest a slightly lower partial volumes of hydrotropes in their aggregated state than those of typical surfactants in their micellar state. This further implies that in the aggregated state hydrotropes have a slightly more close-packed structure. With increasing temperature there is a loss of hydrophobic hydration (which we have elaborately discussed later) of the monomers due to the formation of aggregated structure. As a result, the value of ΔV_m at higher temperature decreases. Again, weakening of hydrogen bonds among water molecules around the small tail part of SCS molecules at higher temperature can further reduce the hydrophobic hydration, which indirectly affects the value of ΔV_m . Moreover, we estimated the value of osmotic coefficients (ϕ) for different solutions and in Figure 3; the same are plotted as a function of solute concentrations. In the inset of the same Figure, we have shown the available experimental osmotic coefficient values for different systems.²⁶ As concentration of SCS increases, the formation of aggregates (due to solute–solute interactions) leads to a decrease in the ϕ value.^{48,49} The effect of temperature on the aggregation propensity of SCS is also quite evident. In brief, because the aggregation propensity of SCS increases with temperature, for a fixed concentration, we observe

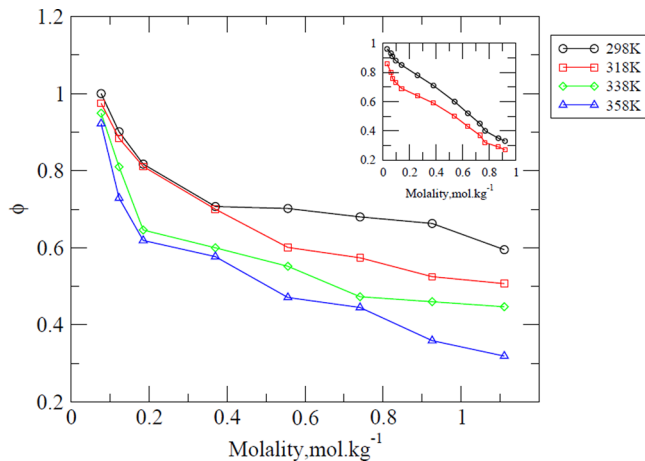


Figure 3. Osmotic coefficients (ϕ) versus SCS concentration for different temperatures. The data in the inset represent the experimental osmotic coefficient values taken from ref 26.

a reduction in the ϕ value at higher temperature. In this context it is worth noting that although at preaggregation regions the estimated values of ϕ are in good agreement with that of experimental findings, in the postaggregation regions they differ modestly.²⁶ The higher osmotic coefficient values in concentrated solution, as estimated here, suggest that the model SCS considered in this study shows less aggregation tendency.

B. Solution Structural Properties. To obtain in detail structural properties of different solutions, we consider selected site–site rdf's involving hydrotrope and water molecules. These distribution functions are shown in Figures 4, 5, 7, 9, and 10.

To get an idea about the aggregation behavior of the hydrotrope through its hydrophobic tail, we first consider distribution functions between C_7-C_7 and C_8-C_8 atoms of SCS with varying concentration and temperature. These rdf's are presented in Figures 4 and 5. Considering C_7-C_7 rdf first, we observe that a strong first peak appears at ~ 5.45 Å. Furthermore, at a particular temperature as the SCS concentration increases, there is an increase in the first peak height (Figure 4i). Here we note that due to use of small number of SCS molecules in systems S0 and S1 the peaks are a bit noisy. Moreover, keeping the concentration at a fixed value we notice a diminution of the first peak height with the decrease in temperature for all of the systems except for systems S0 and S1. Note that these systems are below the MHC level and they belong to preaggregated regions. For C_8-C_8 correlation function (Figure 5), the effect of solute concentration and temperature on it is very similar to that of C_7-C_7 distribution functions. Note that solute–solute rdf's involving other SCS atoms are not shown because they show very little or no concentration and temperature dependency. These observations indicate an enhancement in the solute–solute interactions through nonpolar C_7 and C_8 atomic sites of SCS with increasing concentration and temperature. The temperature and hydrotrope concentration induced aggregation of SCS

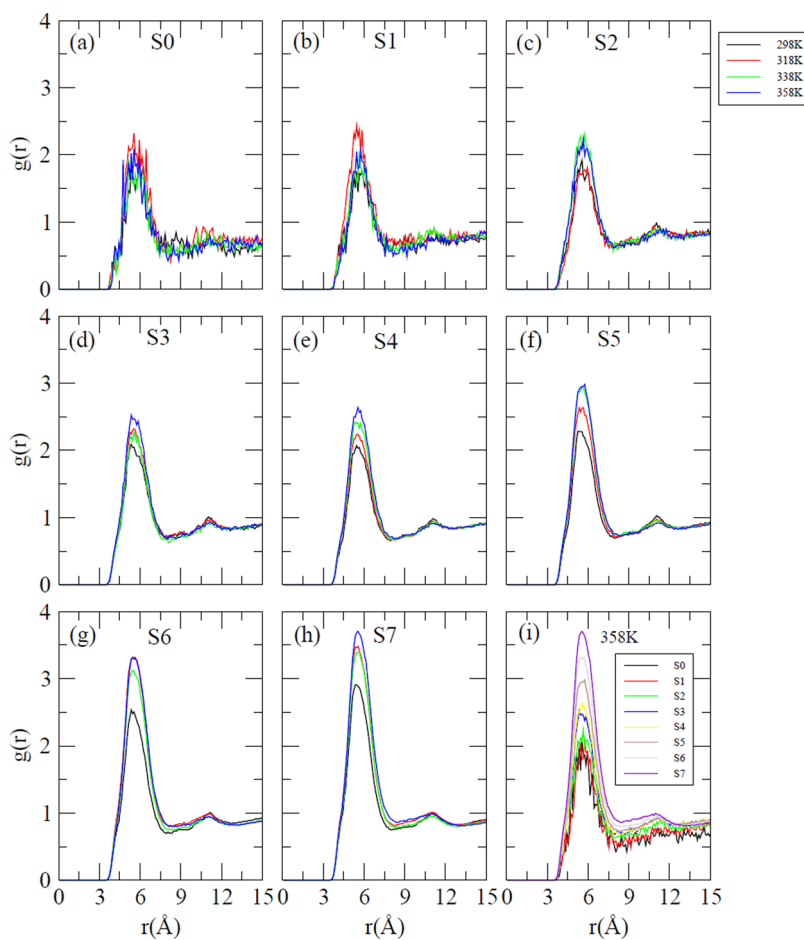


Figure 4. C_7-C_7 site–site radial distribution functions for different systems (a–h). (i) Change in C_7-C_7 rdf with increasing SCS concentration at temperature 358 K.

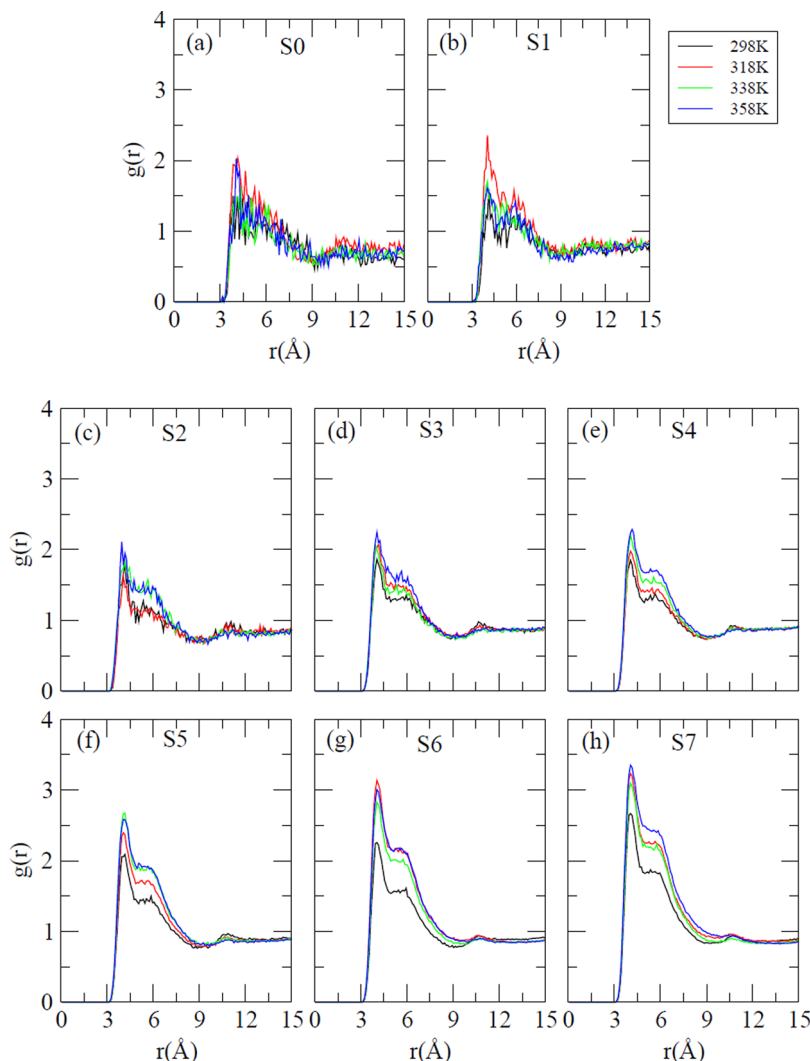


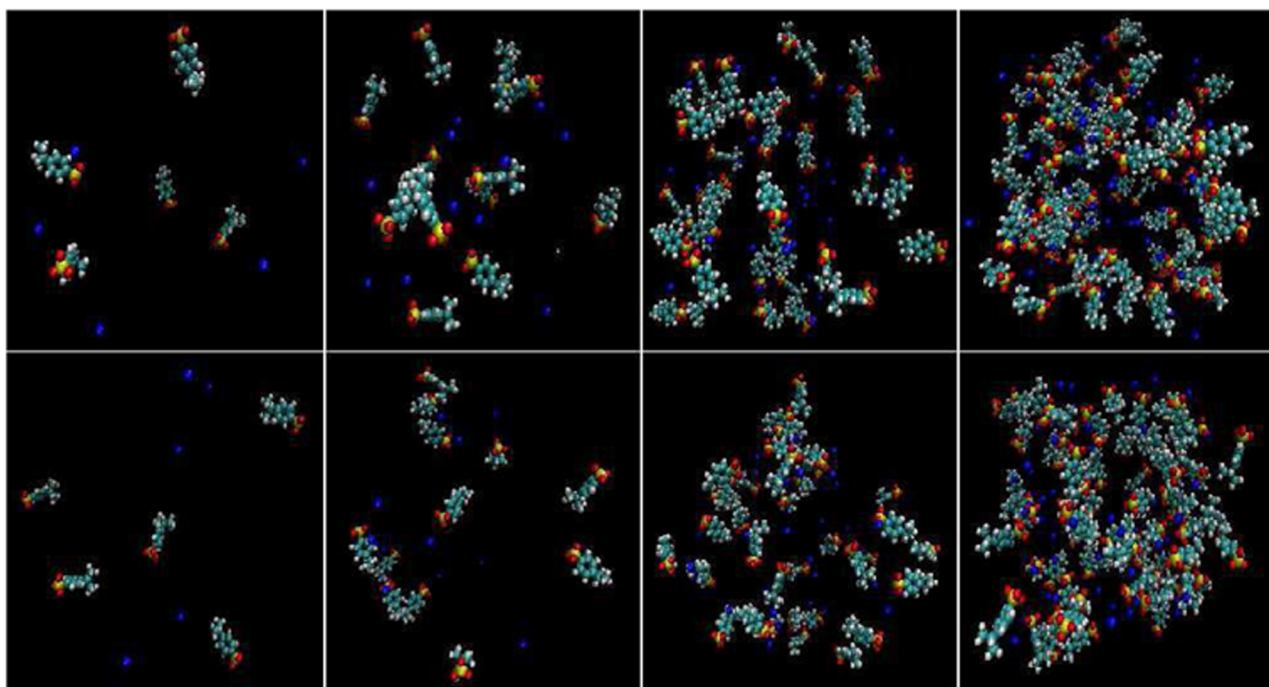
Figure 5. C_8-C_8 site–site radial distribution functions for different systems.

molecules are further probed by visualizing snapshots of different systems taken at the end of each simulation. In Figure 6a we present the snapshots for systems S0, S2, S4, and S7 for 298 and 358 K temperatures considering SCS molecules only. To have proper visual clarity, water molecules and other systems are left off. We chose the systems in such a manner that the concentration of SCS falls below MHC level for one system (i.e., system S0), significant changes in the apparent and partial molal volumes take place for two systems (i.e., systems S2 and S4), and the concentration of SCS is above MHC level for one system (i.e., system S7). As can be seen, the formation of aggregates of SCS molecules is absent below MHC level (S0), whereas it starts appearing for system S2. For other systems, the presence of a substantial amount of SCS aggregates is quite visible. Furthermore, a close examination of SCS clustering reveals that it is the hydrophobic tail that contributes to the SCS aggregation (Figure 6b).

Because the self-aggregation propensity of solute SCS molecules in water is reflected in the hydration pattern, we further extend our study to a close examination of distribution functions involving the C_7 atom of SCS and water molecules. Figure 7a–h displays the rdf's between the C_7 atom of SCS and the oxygen atom of water. Note that the oxygen atom of water is abbreviated here by O_w . Concentrating on the hydration of C_7

atom of SCS at 298 K first (Figure 7a), we make the following observations: (a) The rdf starts to rise at 3.05\AA and reaches the bulk value (where $g(r) = 1$) at $\sim 4.25 \text{\AA}$. Hence, below 4.25\AA there is an exclusion of water molecules from the solvation shell of C_7 atoms. (b) The minimum of the first peak position that appears at 6.15\AA indicates the outer limit of first hydration shell of C_7 atom of SCS. (c) The $g(r)$ value of the S0 system is 1.40 at the first maximum, implying that the first peak water density is only 1.40 times that of bulk density. The effect of temperature on this rdf is also quite visible. In brief, for a fixed SCS concentration, increasing temperature causes a depletion in the first peak height. Although this effect is not very remarkable for systems with low SCS concentrations, we do observe a modest change in the first peak height for concentrated solution systems. Furthermore, increased temperature makes the first valley shallower. In regard to the effect of SCS concentration on C_7-O_w distribution function, we find that on addition of SCS the first peak decreases modestly, especially for concentrated SCS solution systems. These observations imply increased SCS concentration, and elevation of temperature causes a reduction in the number of water molecules in the first solvation shell of C_7 atom of SCS. To verify this we have further estimated the number of water molecules in the solvation shell of hydrophobic C_7 (and C_8) atom by using eq 3.

(a)



(b)

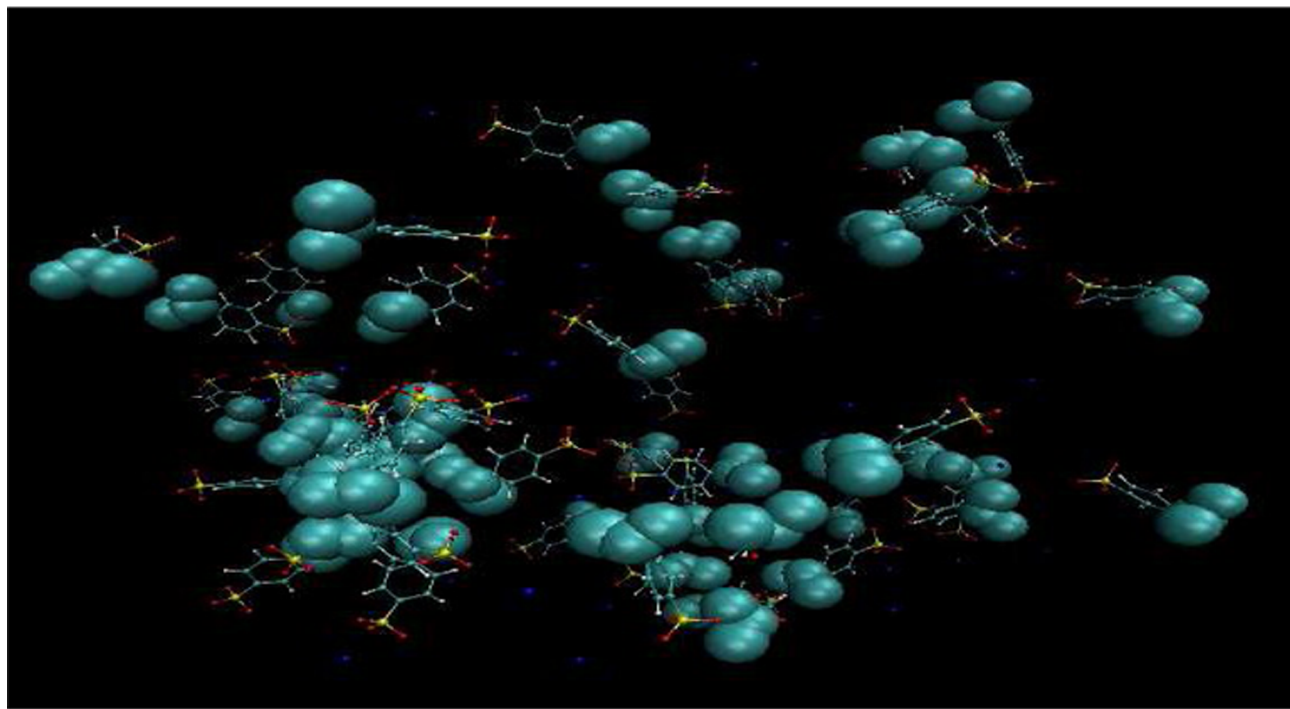


Figure 6. (a) Snapshots of SCS aggregation for systems S0, S2, S4, and S7 (from left to right) for 298 and 358 K temperature (top to bottom). Blue balls represent sodium ions. (b) Close view of clustering of SCS molecules through hydrophobic tail (represented by green balls). The system considered is S5 at 338 K temperature. For both snapshots, water molecules are left off to have proper visual clarity.

$$n_{\alpha\beta} = 4\pi\rho_\beta \int_{r_1}^{r_2} r^2 g_{\alpha\beta}(r) dr \quad (3)$$

where $n_{\alpha\beta}$ represents the number of atoms of type β surrounding atom α in a shell extending from r_1 to r_2 and ρ_β is the number density of β in the system. Typical values for r_1 and r_2 are set to

zero and the distance of the first minimum in the corresponding distribution function, respectively, to calculate the first solvation shell coordination number.

Tables 2 and 3 display the number of water molecules that are present in the first solvation shell of C_7 and C_8 atomic sites of SCS. As can be seen, for a fixed temperature the number of first-

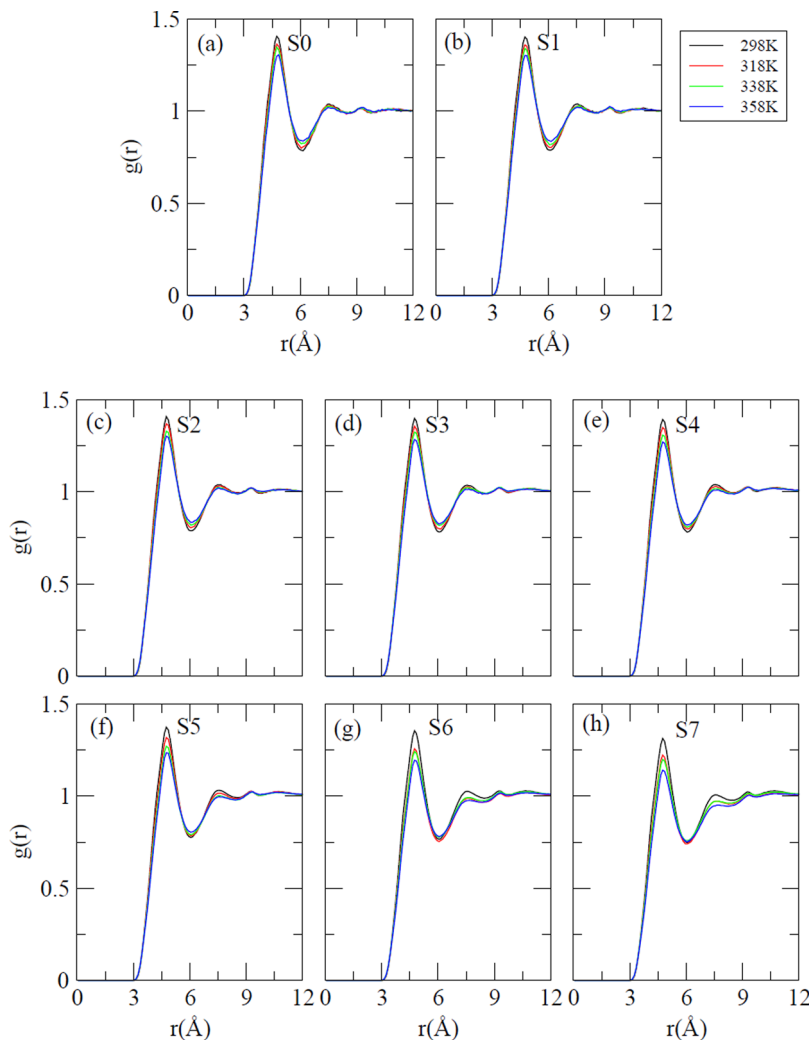


Figure 7. Site–site radial distribution functions between C_7 – O_w .

Table 2. Number of First-Shell Water Molecules around C_7 Atom of Sodium Cumene Sulfonate Molecules^a

system	298 K	318 K	338 K	358 K
S0	30.32	29.75	29.15	28.47
S1	29.83 (30.11)	29.03 (29.49)	28.66 (29.00)	28.06 (28.26)
S2	29.13 (30.00)	28.67 (29.18)	27.79 (28.86)	27.21 (27.98)
S3	27.06 (29.17)	26.32 (28.62)	25.98 (28.23)	25.11 (27.27)
S4	25.46 (28.41)	24.72 (27.84)	24.02 (27.31)	23.32 (26.55)
S5	23.53 (27.84)	22.63 (27.24)	21.84 (26.72)	21.30 (26.01)
S6	21.82 (27.12)	20.31 (26.46)	20.19 (26.09)	19.42 (25.23)
S7	20.02 (26.47)	18.67 (25.92)	18.40 (25.50)	17.56 (24.73)

^aValues in the parentheses represent the first-shell coordination number if the only change with added SCS came through the number density change.

shell water molecules around C_7 (and C_8) atom decreases as the concentration of SCS is increased. Note that we have added SCS molecules without replacing water molecules. As a result the box volume increases as one moves from system S0 to system S7, which makes the water number density lower. So, a decrease in the coordination number value is expected because of this change in the box volume. In an attempt to nullify the effect of increased box volume on the coordination number value, we normalized the coordination number value of different systems such that the change in its value purely reflects the effect of added hydrotropes and these normalized coordination number values are also

included in the parentheses of the same Tables. For systems up to 0.185*m* concentration we observe very little change in the coordination number value, whereas a marked change in its number is observed above this concentration. These observations hold true for all temperatures considered in this study. The effect of increased temperature is also quite evident from these Tables. In specific, as temperature increases we observe a modest decrease in the coordination number value. In view of these, by using the VMD program we have further carried out the atomic mass density analysis. Figure 8 represents the mass density map of oxygen atom of water with a cell side of 0.5 Å within 4.75 Å

Table 3. Number of First-Shell Water Molecules around C₈ Atom of Sodium Cumene Sulfonate Molecules^a

system	298 K	318 K	338 K	358 K
S0	16.53	16.11	15.78	15.32
S1	16.37 (16.42)	15.85 (15.97)	15.56 (15.70)	15.17 (15.21)
S2	16.06 (16.35)	15.74 (15.80)	15.22 (15.62)	14.82 (15.06)
S3	15.20 (15.90)	14.72 (15.50)	14.45 (15.28)	13.92 (14.67)
S4	14.51 (15.49)	14.06 (15.08)	13.58 (14.78)	13.12 (14.29)
S5	13.63 (15.18)	13.05 (14.75)	12.53 (14.46)	12.17 (14.00)
S6	12.83 (14.78)	11.83 (14.33)	11.71 (14.12)	11.20 (13.58)
S7	11.88 (14.43)	10.99 (14.04)	10.79 (13.80)	10.21 (13.30)

^aValues in the parentheses represent the first-shell coordination number if the only change with added SCS came through the number density change.

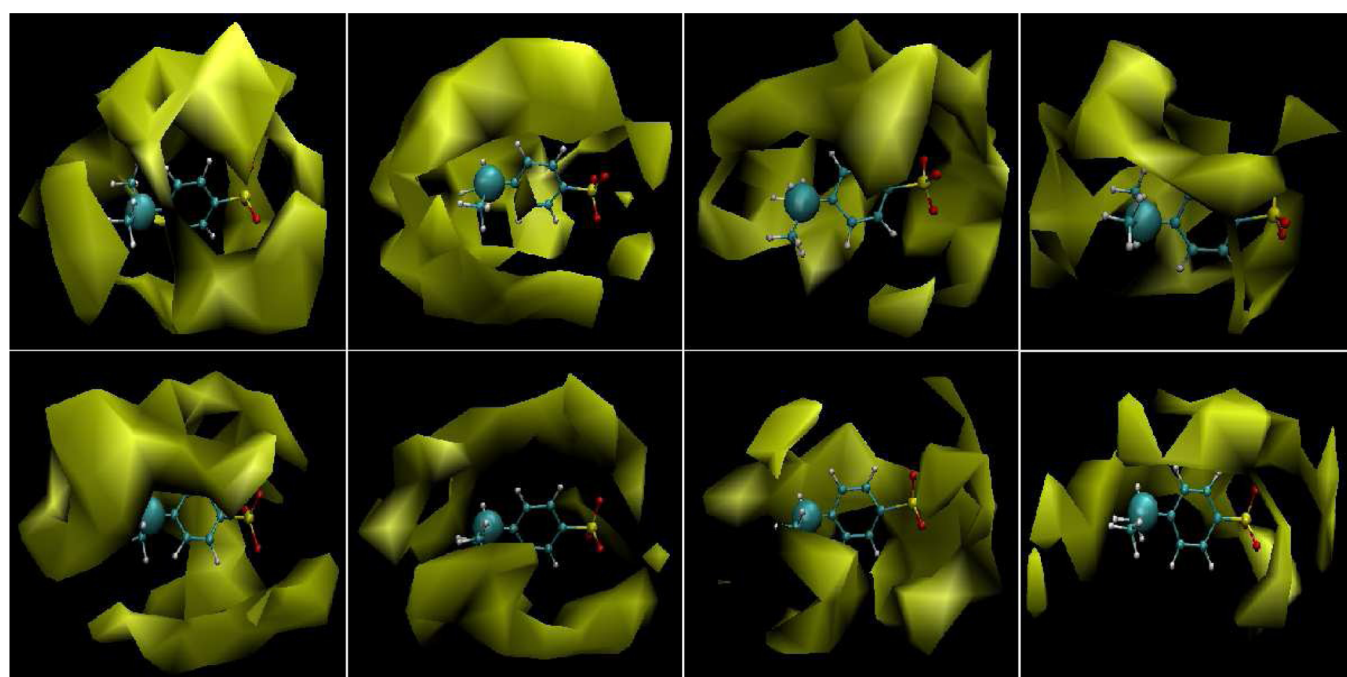


Figure 8. Contours of solvent water density within 4.75 Å around C₇ atom (large green ball) of a randomly chosen SCS molecule at different time intervals. From left to right: 0, 10, 20, and 40 ns. Top: at 298 K; bottom: at 358 K.

(the position of first peak maximum of C₇–O_w distribution function) around the C₇ atom of a randomly chosen SCS molecule at different time intervals. For this, we have considered system S3 for two different temperatures (298 and 358 K). Note that in the starting configuration all SCS molecules are dispersed in the solution, and as the simulation progresses the aggregation of SCS molecules takes place. This can be clearly interpreted from this Figure. At the beginning of the simulation, we observe a very high water density around the SCS molecule, and as soon as aggregates begin to form, a clear depletion in the water density around the C₇ atom is observed. The effect of temperature is also quite apparent. In brief, as temperature increases a lowering of the water density at 358 K (compared with that at 298 K) is also noticed. These facts suggest that elevation in temperature causes an exclusion of more number water molecules from the solvation shell of hydrophobic tail of SCS. These findings also act as corroborative evidence of what we observe in the C₇–C₇ and C₇–O_w distribution functions.

To investigate the influence of hydrotrope concentration and the effect of temperature on the water structure, we consider water oxygen–water oxygen (O_w–O_w) rdf's of different systems (Figure 9). It is important to examine the water–water

distribution function because it provides, albeit indirectly, the details of the solvation of hydrotrope SCS. The first and second peak of the O_w–O_w distribution function that appears at 2.75 and 4.55 Å corresponds to the H-bonded first neighbor and the tetrahedrally located second neighbor, respectively. We note that the location of these peaks in the O_w–O_w rdf's resembles well that already reported elsewhere.⁵⁰ As we move from low to high SCS concentration, although a negligibly small enhancement in the first peak height of the O_w–O_w distribution function is observed the first valley becomes shallower and the second peak becomes less pronounced. These suggest some perturbations of tetrahedrally located water structure at higher SCS concentrations. Taking into consideration the effect of temperature at a fixed SCS concentration, we find that the locations of the first and second peak remain unaltered with increasing temperature. However, a depletion in the first and second peak height and a much shallower first valley are observed as the temperature is increased. These results indicate that both increased concentration and elevated temperature bring about the same effect in regards to changes in water structure. The only difference is that the temperature affects both the H-bonded first neighbor and the tetrahedrally located second neighbor, while a change in SCS

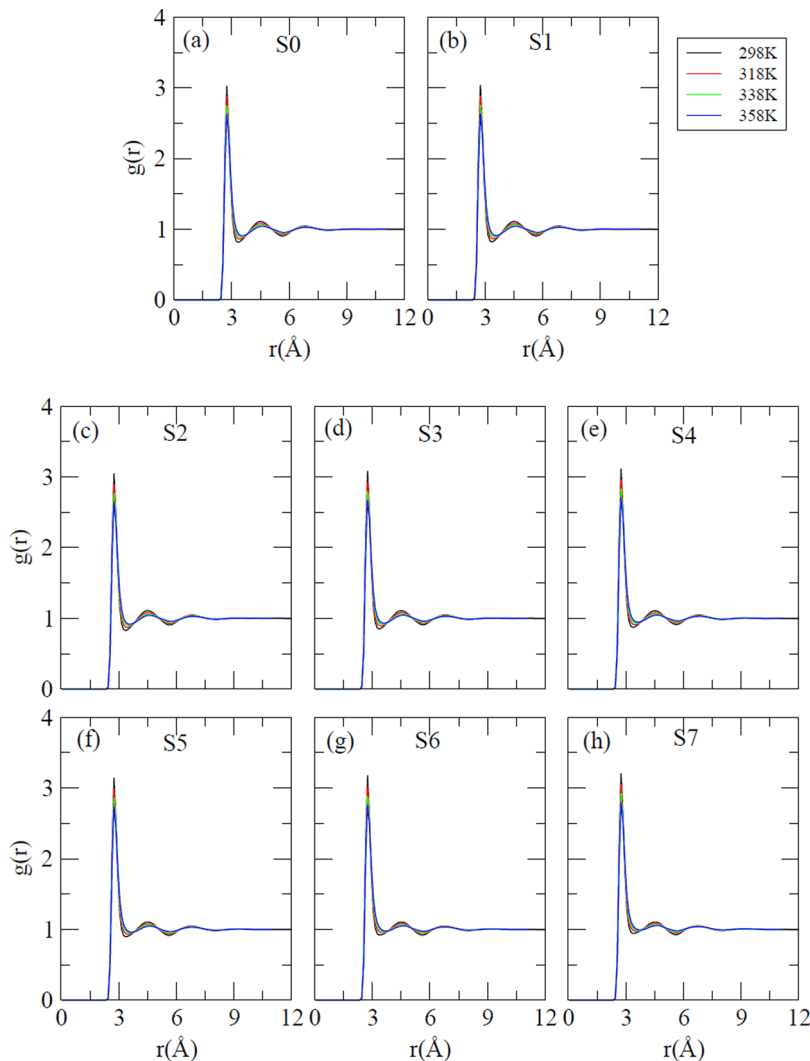


Figure 9. Site–site radial distribution functions between $O_w - O_w$.

concentration affects only the tetrahedrally located water structure.

Because the pair correlation function provides information about the probability density distribution of the atoms around a particular site, it is instructive to determine the probability of counterion (Na^+) density around the polar charged site (O atom attached to the sulfur atom) of the sulfonate anion. The rdf's for polar headgroup and counterion ($O - Na^+$) for different systems are presented in Figure 10. Examining the polar headgroup and counterion rdf, we observe that it is a bimodal type distribution with the peaks appearing at 2.35 and 4.65 Å, respectively. Unlike unimodal distribution, a bimodal distribution identifies the advent of a dual charge layer around the polar headgroup at two radial locations in space. Although Na^+ ions are attached within the Stern layer of the aggregated systems, they are not able to screen the effect of charged surface completely. In regard to the effect of temperature at a fixed SCS concentration we find that the height of both of these peaks is slightly enhanced as temperature increases (except for systems S0 and S1). Although the addition of SCS causes a small depletion in the first peak height and an enhancement in the second peak height for all systems considered here except for the S0 and S1 systems (which are below MHC level), these are not a strong function of SCS concentration. Nevertheless, these results suggest the enhance-

ment in dual charge layer as the self-aggregation of hydrotropes increases.

C. Hydrogen-Bond Properties. Because of the presence of oxygen atoms in the sulfonate group of SCS, in aqueous solution it has an ability to act as a hydrogen bond acceptor and forms hydrogen bonds with water molecules. Water structure can be affected by these hydrogen bonds, which can also promote extensive concentration and temperature-dependent aggregation of hydrotropes. Note that because a SCS molecule cannot form hydrogen bonds with like molecules, in aqueous SCS solution two different types of hydrogen bonds are possible, namely, water–water and water–SCS hydrogen bonds. In view of this, following previous works,^{51–53} we have estimated the average number of hydrogen bonds of each of these types by considering certain geometric criterion. If interatomic distance between hydrotrope oxygen and water oxygen is <3.15 Å and simultaneously the $O-O-H$ angle is $<45^\circ$, then these two molecules are considered to be hydrogen-bonded. In the case of the water–water hydrogen bond the cutoff distance is <3.35 Å and the angle is the same as that of the water–SCS hydrogen bond. The cutoff distances of these hydrogen bonds are determined from the position of first minimum of the corresponding rdf's. In this context, it is worth noting that the formation of hydrogen bonds between hydrotrope and water

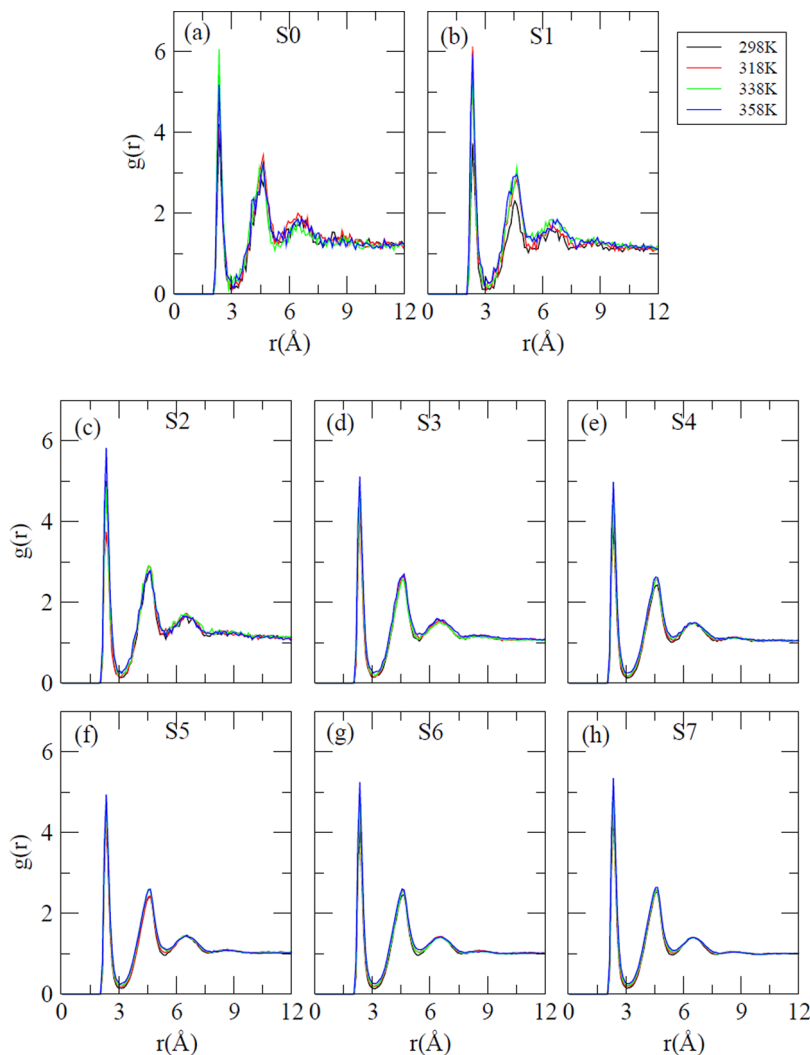


Figure 10. Site–site radial distribution functions between oxygen atom of polar headgroup of SCS and Na^+ ion.

molecules depends on the availability of the polar headgroup of SCS for water. If the aggregation of SCS molecules makes its sulfonate group less accessible (due to overlapping of nonpolar and polar groups of SCS) for water molecules to form intermolecular water–SCS hydrogen bonds, then we would observe a depletion in the average number of these hydrogen bonds above MHC level. If the formation of SCS aggregates takes place in such a manner that the availability of its polar sulfonate group is not affected much, then one can expect “no impact” of SCS aggregate formation on the water–SCS hydrogen bond number. In Tables 4 and 5 the average number of hydrogen bonds between water–water and water–SCS (per SCS) for all systems are presented. As per the expectation, temperature-induced breaking of some of the water–water and water–SCS hydrogen bonds causes a depletion in the values of average number of hydrogen bonds. In regard to the effect of added hydrotropes on water–water and water–SCS hydrogen bond numbers, we notice that as concentration increases the values of both of them decrease. Because SCS molecules are capable of hydrogen-bond formation with water (due to the presence of three oxygen atoms in the polar headgroup), some of the water–water hydrogen bonds are replaced by water–SCS hydrogen bonds. As a result, the average number of water–water hydrogen bonds diminishes. For, water–SCS per SCS hydrogen bonds,

Table 4. Average Number of Water–Water (per Water) Hydrogen Bonds for Different Systems

system	$\text{HB}_{\text{water-water}}$			
	298 K	318 K	338 K	358 K
S0	3.23	3.14	3.05	2.96
S1	3.22	3.13	3.04	2.94
S2	3.21	3.11	3.02	2.93
S3	3.16	3.07	2.98	2.89
S4	3.11	3.03	2.94	2.85
S5	3.07	2.98	2.90	2.81
S6	3.03	2.94	2.85	2.76
S7	2.98	2.90	2.81	2.73

with increasing concentration because the number of hydrotropes molecules increases (keeping the number of solvent water remains unchanged), we observe a modest decrease in the average number of this type of hydrogen bond, although the total number of water–SCS hydrogen bonds in the system increases on addition of SCS molecules. Here we note that we did not notice any sharp change in either of these two hydrogen bonds at (and above) MHC level. So at this point it is safe to conclude that it is the hydrophobic tail group of hydrotropic SCS through which the formation of SCS aggregates takes place. Moreover, in the

Table 5. Average Number of SCS–Water (per SCS) Hydrogen Bonds for Different Systems

system	HB _{SCS–water}			
	298 K	318 K	338 K	358 K
S0	4.74	4.67	4.50	4.33
S1	4.73	4.54	4.41	4.32
S2	4.62	4.53	4.38	4.30
S3	4.64	4.49	4.36	4.25
S4	4.62	4.47	4.35	4.19
S5	4.57	4.45	4.31	4.17
S6	4.57	4.40	4.29	4.12
S7	4.50	4.36	4.24	4.09

aggregates the accessibility of the polar hydrogen bonding group of a SCS molecule for water remains essentially unaffected.

IV. SUMMARY AND CONCLUSIONS

Employing classical molecular dynamics simulations, we have investigated the molecular mechanisms of self-aggregation behavior of hydrotrope SCS in aqueous solutions. Eight different SCS concentrations and, for each SCS concentration, four different temperatures have been considered. We also compared our findings with the available experimental results wherever it was necessary. From the calculations of apparent and partial molal volumes of SCS at different concentrations we observed a sudden and dramatic change in the solution structures up to MHC of SCS. In brief, the self-aggregation of SCS molecules starts at 0.185m, and with increasing concentration the growth of SCS molecules leads to an increase in apparent and partial molal volumes of SCS, but above 0.370m concentration the change in these quantities is not very dramatic, suggesting that above this concentration although the number of SCS aggregates in the system increases the size of them does not. Note that the change in the apparent and partial molal volume of SCS with concentrations estimated in this study is in accordance with the experimental findings, albeit qualitatively. Furthermore, in comparison with the typical surfactants, the volume change accompanying the aggregation of SCS is slightly lower, indicating a slightly more closed-packed structure of SCS aggregates. The formation of hydrotrope clusters above MHC is further probed by the estimation of osmotic coefficients value for different systems. Furthermore, in contrast with the experimental findings,²⁶ our calculated molal expansibility at infinite dilution value suggests the water structure breaking ability of SCS molecules.

To examine the origin of SCS aggregate formation above MHC level, we considered different site–site distribution functions of water and SCS molecules. At a fixed temperature, on addition of SCS we found the dehydration of hydrophobic tail of SCS, and the effect is very pronounced above the MHC level. This observation is further confirmed by the atomic mass density analysis. This suggests that it is the interaction between the hydrophobic tails of different SCS molecules that contributes to SCS aggregate formation. The effect of elevated temperature on this dehydration process is also quite visible. As temperature increases, we observed more and more exclusion of water molecules from the hydrophobic atomic sites of SCS, and as a result the aggregation of SCS increases. Interestingly, as suggested by hydrogen-bond analysis, the formation of aggregates does not have much influence on the average number of water–SCS hydrogen bonds, indicating that the accessibility of polar sulfonate headgroup of SCS for water molecules is not

greatly affected. Furthermore, a bimodal type distribution is also observed from the calculation of pair correlation function involving the polar headgroup oxygen of SCS and sodium ion. This suggests the presence of a dual charge layer around the polar headgroup of SCS at two radial distances, and this dual charge layer becomes enhanced as self-aggregation of SCS increases.

■ AUTHOR INFORMATION

Corresponding Author

*E-mail: sandipp@iitg.ernet.in.

Notes

The authors declare no competing financial interest.

■ ACKNOWLEDGMENTS

Part of the research was enabled using the computation facility of C-DAC, Pune India.

■ REFERENCES

- (1) Neuberg, C. Über Hydrotropie. *Biochem. Z.* **1916**, *76*, 107–176.
- (2) Hodgdon, T. K.; Kaler, E. W. Hydrotropic Solutions. *Curr. Opin. Colloid Interface Sci.* **2007**, *12*, 121–128.
- (3) Subbarao, C. V.; Chackravarthy, I. P. K.; Sai Bharadwaj, A. V. S. L.; Prasad, K. M. M. Functions of Hydrotropes in Solutions. *Chem. Eng. Technol.* **2012**, *35*, 225–237.
- (4) Saleh, A. M.; Elkhordegui, L. K. Hydrotropic Agents—A New Definition. *Int. J. Pharm.* **1985**, *24*, 231–238.
- (5) Heldt, N.; Zhao, J.; Friberg, S.; Zhang, Z.; Slack, Y.; Li, Y. Controlling the Size of Vesicles Prepared from Egg Lecithin Using a Hydrotrope. *Tetrahedron* **2000**, *56*, 6985–6990.
- (6) Friberg, S. E.; Yang, J.; Huang, T. A Reversible Extraction Process of Phenethyl Alcohol, A Fragrance. *Ind. Eng. Chem. Res.* **1996**, *35*, 2856–2859.
- (7) Guo, R.; Zhang, Q.; Qian, J.; Zou, A. Hydrotropic and Hydrotropic–Solubilization Action of Penicillin-K in CTAB/n-C₈H₁₇OH/H₂O System. *Colloids Surf., A* **2002**, *196*, 223–224.
- (8) Woolfson, A. D.; McCafferty, D. F.; Launchbury, A. P. Stabilisation of Hydrotropic Temazepam Parenteral Formulations by Lyophilisation. *Int. J. Pharm.* **1986**, *34*, 17–22.
- (9) Jain, N. K.; Patel, V. V.; Taneja, L. N. Formulation and Evaluation of Nifedipine Injection. *Pharmazie* **1988**, *43*, 254–255.
- (10) Osborne, D. W. The Effect of the Monosodium Salt of a C₂₁ Dicarboxylic Acid Hydrotrope on Biosurfactant bilayers: Transdermal Delivery Considerations. *Colloids Surf. A* **1988**, *30*, 13–23.
- (11) Koparkar, Y. P.; Gaikar, V. G. Solubility of o-/p-Hydroxyacetophenones in Aqueous Solutions of Sodium Alkyl Benzene Sulfonate Hydrotropes. *J. Chem. Eng. Data* **2004**, *49*, 800–803.
- (12) Gaikar, V. G.; Sharma, M. M. Extractive Separation with Hydrotropes. *Solvent Extr. Ion Exch.* **1986**, *4*, 839–846.
- (13) Agarwal, M.; Gaikar, V. G. Extractive Separation Using Hydrotropes. *Sep. Technol.* **1992**, *2*, 79–84.
- (14) Mahapatra, A.; Gaikar, V. G.; Sharma, M. M. New Strategies in Extractive Distillation: Use of Aqueous Solutions of Hydrotropes and Organic Bases as Solvent for Organic Acids. *Sep. Sci. Technol.* **1988**, *23*, 429–435.
- (15) Raney, K. H.; Miller, C. A. Optimum Detergency Conditions with Nonionic Surfactants: II. Effect of Hydrophobic Additives. *J. Colloid Interface Sci.* **1987**, *119*, 539–549.
- (16) Dandekar, D. V.; Gaikar, V. G. Hydrotropic Extraction of Curcuminoids from Turmeric. *Sep. Sci. Technol.* **2003**, *38*, 1185–1215.
- (17) Raman, G.; Gaikar, V. G. Extraction of Piperine from Piper Nigrum (Black Pepper) by Hydrotropic Solubilization. *Ind. Eng. Chem. Res.* **2002**, *41*, 2966–2976.
- (18) Stylian, G. E.; Bramhall, A. E. Lignin Solvation Improves Mechanical Pulp Processing. *Pulp Pap. Can.* **1979**, *80*, 74–77.
- (19) Schobert, B. The Anomalous Colligative Properties of Proline. *Naturwissenschaften* **1977**, *64*, 386.

- (20) Balasubramanian, D.; Friberg, S. E. In *Surface and Colloid Science*; Matijevic, E., Ed.; Plenum Press: New York, 1993; Vol. 15.
- (21) *Amphoteric Surfactants*, 2nd ed.; Lomax, E. G., Ed.; Marcel Dekker, Inc: New York, 1996.
- (22) Danielson, I.; Stenius, P. Anion Association and Micelle Formation in Solutions of Hydrotropic and Short-Chain Carboxylates. *J. Colloid Interface Sci.* **1971**, *37*, 264–280.
- (23) Hopkins Hatzopoulos, M.; Eastoe, J.; Dowding, P. J.; Rogers, S. E.; Heenan, R. K.; Dyer, R. Are Hydrotropes Distinct from Surfactants? *Langmuir* **2011**, *27*, 12346–12353.
- (24) Kim, J. Y.; Kim, S.; Papp, M.; Park, K.; Pinal, R. Hydrotropic Solubilization of Poorly Water-Soluble Drugs. *J. Pharm. Sci.* **2010**, *99*, 3953–3965.
- (25) Bauduin, P.; Renoncourt, A.; Kopf, S.; Touraud, D.; Kunz, W. Unified Concept of Solubilization in Water by Hydrotropes and Cosolvents. *Langmuir* **2005**, *21*, 6769–6775.
- (26) Wagle, V. B.; Kothari, P. S.; Gaikar, V. G. Effect of Temperature on Aggregation Behavior of Aqueous Solutions of Sodium Cumene Sulfonate. *J. Mol. Liq.* **2007**, *133*, 68–76.
- (27) Balasubramanian, D.; Srinivas, V. When Does the Switch from Hydrotropy to Micellar Behavior Occur? *Langmuir* **1998**, *14*, 6658–6661.
- (28) Sadvilkar, V. G.; Samant, S. D.; Gaikar, V. G. Claisen-Schmidt Reaction in a Hydrotropic Medium. *J. Chem. Technol. Biotechnol.* **1995**, *62*, 405–410.
- (29) Balasubramanian, D.; Srinivas, V.; Gaikar, V. G.; Sharma, M. M. Aggregation Behavior of Hydrotropic Compounds in Aqueous Solution. *J. Phys. Chem.* **1989**, *93*, 3865–3870.
- (30) Booth, J. J.; Abbott, S.; Shimizu, S. Mechanism of Hydrophobic Drug Solubilization by Small Molecule Hydrotropes. *J. Phys. Chem. B* **2012**, *116*, 14915–14921.
- (31) Bauduin, P.; Testard, F.; Zemb, Th. Solubilization in Alkanes by Alcohols as Reverse Hydrotropes or “Lipotropes”. *J. Phys. Chem. B* **2008**, *112*, 12354–12360.
- (32) Neumann, M. G.; Schmitt, C. C.; Prieto, K. R.; Goi, B. E. The Photophysical Determination of the Minimum Hydrotrope Concentration of Aromatic Hydrotropes. *J. Colloid Interface Sci.* **2007**, *315*, 810–813.
- (33) Hassan, P. A.; Raghavan, S. R.; Kaler, E. W. Microstructural Changes in SDS Micelles Induced by Hydrotropic Salt. *Langmuir* **2002**, *18*, 2543–2548.
- (34) Case, D. A.; Darden, T. A.; Cheatham, III, T. E.; Simmerling, C. L.; Wang, J.; Duke, R. E.; Luo, R.; Walker, R. C.; Zhang, W.; Merz, K. M.; et al. AMBER 12; University of California, San Francisco, 2012.
- (35) Berendsen, H. J. C.; Grigera, J. R.; Straatsma, T. P. The Missing Term in Effective Pair Potentials. *J. Phys. Chem.* **1987**, *91*, 6269–6271.
- (36) Vanommeslaeghe, K.; Hatcher, E.; Acharya, C.; Kundu, S.; Zhong, S.; Shim, J.; Darian, E.; Guvench, O.; Lopes, P.; Vorobyov, I.; MacKerell, A. D., Jr. CHARMM General Force Field: A Force Field for Drug-Like Molecules Compatible with the CHARMM All-Atom Additive Biological Force Fields. *J. Comput. Chem.* **2010**, *31*, 671–690.
- (37) e, X.; Guvench, O.; MacKerell, A. D.; Klein, M. L. Atomistic Simulation Study of Linear Alkylbenzene Sulfonates at the Water/Air Interface. *J. Phys. Chem. B* **2010**, *114*, 9787–9794.
- (38) Mark, P.; Nilsson, L. Structure and Dynamics of the TIP3P, SPC, and SPC/E Water Models at 298 K. *J. Phys. Chem. A* **2001**, *105*, 9954–9960.
- (39) Crowley, M. F.; Williamson, M. J.; Walker, R. C. CHAMBER: Comprehensive Support for CHARMM Force Fields Within the AMBER Software. *J. Comput. Chem.* **2009**, *109*, 3767–3772.
- (40) Martinez, L.; Andrade, R.; Birgin, E. G.; Martinez, J. M. PACKMOL: A Package for Building Initial Configurations for Molecular Dynamics Simulations. *J. Comput. Chem.* **2009**, *30*, 2157–2164.
- (41) Berendsen, H. J. C.; Postma, J. P. M.; van Gunsteren, W. F.; DiNola, A.; Haak, J. R. Molecular Dynamics with Coupling to an External Bath. *J. Chem. Phys.* **1984**, *81*, 3684–3690.
- (42) Ryckaert, J. P.; Ciccotti, G.; Berendsen, H. J. C. Numerical Integration of the Cartesian Equations of Motion of a System with Constraints: Molecular Dynamics of n-Alkanes. *J. Comput. Phys.* **1977**, *23*, 327–341.
- (43) Humphrey, W.; Dalke, A.; Schulter, K. VMD: Visual Molecular Dynamics. *J. Mol. Graphics* **1996**, *14*, 33–38.
- (44) Wandrey, C.; Bartkowiak, A.; Hunkeler, D. Partial Molar and Specific Volumes of Polyelectrolytes: Comparison of Experimental and Predicted Values in Salt-free Solutions. *Langmuir* **1999**, *15*, 4062–4068.
- (45) Leduc, P. A.; Fortier, J. L.; Desnoyers, J. E. Apparent Molal Volumes, Heat Capacities, and Excess Enthalpies of n-Alkylamine Hydrobromides in Water As a Function of Temperature. *J. Phys. Chem.* **1974**, *78*, 1217–1225.
- (46) Goolam, M. M.; Gerald, P.; Jacques, E. D. The effect of Temperature and Urea on the Apparent Molal Volumes and Heat Capacities of n-Nonyltrimethylammonium Bromide in Water. *J. Colloid Interface Sci.* **1976**, *54*, 80–93.
- (47) Musbally, M. G.; Perron, G.; Denoyers, J. E. Apparent Molal Volumes and Heat Capacities of Ionic Surfactants in Water at 25°C. *J. Colloid Interface Sci.* **1974**, *48*, 494–501.
- (48) Gaikar, V. G.; Wagle, V. B. Osmotic and Activity Coefficients of Short Chain Alkyl Benzene Sulfonates by Vapor Pressure Osmometry. *J. Chem. Eng. Data* **2006**, *51*, 886–891.
- (49) Sharma, B.; Paul, S. Effects of Dilute Aqueous NaCl Solution on Caffeine Aggregation. *J. Chem. Phys.* **2013**, *139*, 194504-1–194504-10.
- (50) Chowdhury, S.; Chandra, A. Molecular Dynamics Simulations of Aqueous NaCl and KCl Solutions: Effects of Ion Concentration on the Single-Particle, Pair, and Collective Dynamical Properties of Ions and Water Molecules. *J. Chem. Phys.* **2001**, *115*, 3732–3741.
- (51) Luzar, A.; Chandler, D. Effect of Environment on Hydrogen Bond Dynamics in Liquid Water. *Phys. Rev. Lett.* **1996**, *76*, 928–931.
- (52) Chandra, A. Effects of Ion Atmosphere on Hydrogen-Bond Dynamics in Aqueous Electrolyte Solutions. *Phys. Rev. Lett.* **2000**, *85*, 768–771.
- (53) Chandra, A. Dynamical Behavior of Anion-Water and Water-Water Hydrogen Bonds in Aqueous Electrolyte Solutions: A Molecular Dynamics Study. *J. Phys. Chem. B* **2003**, *107*, 3899–3906.